Acetogenic bacteria utilize light-driven electrons as an energy source for autotrophic growth

Sangrak Jin[a,b], Yale Jeon[c], Min Soo Jeon[c], Jongoh Shin[a,b], Yoseb Song[a,b], Seulgi Kang[a,b], Jiyun Bae[a,b], Suhyung Cho[a,b], Jung-Kul Lee[d], Dong Rip Kim[c], and Byung-Kwan Cho[a,b,e,1]

[a]Department of Biological Sciences, Korea Advanced Institute of Science and Technology, 34141 Daejeon, Republic of Korea; [b]Innovative Biomaterials Research Center, KI for the BioCentury, Korea Advanced Institute of Science and Technology, 34141 Daejeon, Republic of Korea; [c]Department of Mechanical Engineering, Hanyang University, 04763 Seoul, Republic of Korea; [d]Department of Chemical Engineering, Konkuk University, 05029 Seoul, Republic of Korea; and [e]Intelligent Synthetic Biology Center, 34141 Daejeon, Republic of Korea

Edited by Caroline S. Harwood, University of Washington, Seattle, WA, and approved January 20, 2021 (received for review October 1, 2020)

Acetogenic bacteria use cellular redox energy to convert CO_2 to acetate using the Wood–Ljungdahl (WL) pathway. Such redox energy can be derived from electrons generated from H_2 as well as from inorganic materials, such as photoresponsive semiconductors. We have developed a nanoparticle-microbe hybrid system in which chemically synthesized cadmium sulfide nanoparticles (CdS-NPs) are displayed on the cell surface of the industrial acetogen *Clostridium autoethanogenum*. The hybrid system converts CO_2 into acetate without the need for additional energy sources, such as H_2, and uses only light-induced electrons from CdS-NPs. To elucidate the underlying mechanism by which *C. autoethanogenum* uses electrons generated from external energy sources to reduce CO_2, we performed transcriptional analysis. Our results indicate that genes encoding the metal ion or flavin-binding proteins were highly up-regulated under CdS-driven autotrophic conditions along with the activation of genes associated with the WL pathway and energy conservation system. Furthermore, the addition of these cofactors increased the CO_2 fixation rate under light-exposure conditions. Our results demonstrate the potential to improve the efficiency of artificial photosynthesis systems based on acetogenic bacteria integrated with photoresponsive nanoparticles.

acetogenic bacteria | artificial photosynthesis | cadmium sulfide nanoparticle | extracellular electron transfer | *Clostridium autoethanogenum*

Acetogenic bacteria can convert one carbon gaseous feedstock, such as carbon monoxide (CO) and carbon dioxide (CO_2), to acetate through the Wood–Ljungdahl (WL) pathway. This unique metabolic pathway makes them attractive biocatalysts for the industrial production of value-added biochemicals from waste gases (1–3). Generally, the WL pathway requires hydrogen (H_2) to reduce CO_2 in the form of a redox energy source in acetogenic bacteria. To increase its metabolic capability, numerous efforts have been made to use alternative types of redox energy for CO_2 fixation, such as electricity (4–7). Unlike H_2, the extracellular electrons generated from electricity sources are directly or indirectly transferred into bacterial cells (8, 9). Direct extracellular electron transfer (EET) is a process by which microorganisms get directly attached to the cathode or anode surface to exchange electrons. In contrast, in indirect EET, the specific electron mediators in the extracellular space are reduced by accepting electrons from the electron donors or by donating electrons to the electron carriers in the cytosolic matrix (10–16). Although several studies have shown that acetogenic bacteria can utilize the extracellular electrons directly from electricity sources (4–7), the underlying mechanism of extracellular electron utilization in acetogenic bacteria is elusive.

Several bacterial strains can utilize the redox energy obtained from renewable energy sources, such as sunlight (5, 17–19). For example, biologically synthesized cadmium sulfide (CdS) or gold nanoparticles displaying *Moorella thermoacetica* were tested and found to convert CO_2 to acetate (18, 19). In addition, an artificial photosynthesis system was developed to imitate the Z-scheme of plants through a photocatalytic chain reaction, resulting in the cysteine-CdS-TiO_2 system (20). Based on these developments, two types of EET pathways have been suggested: the H_2 generation pathway by membrane-bound hydrogenase and an H_2-independent pathway (21). In addition, photoresponsive nanoparticles have been attached to the outer membrane of nonacetogenic bacteria, such as yeast or *Escherichia coli*; these systems lead to increased chemical production using light as an energy source (22–24). However, biosynthesis of a photoresponsive CdS leads to a decrease in chemical production because of the heavy metal defense mechanism in bacteria (25, 26). Another limitation is that it is difficult to control the structure or size of the semiconductor to increase the efficiency of electron–hole pair generation.

Here we describe our artificial photosynthesis system developed with chemically synthesized CdS nanoparticles (CdS-NPs) attached to the cell surface of *Clostridium autoethanogenum* DSM 10061, an acetogenic bacterium, and examine whether CO_2 reduction occurs under light-exposure conditions. To understand the underlying metabolism, we also analyze the transcriptome profiles of the CdS-NP-attached *C. autoethanogenum* in response to light exposure.

Significance

To develop an efficient artificial photosynthesis system using acetogen-nanoparticle hybrids, the efficiency of the electron–hole pair generation of nanoparticles must be enhanced to demonstrate extracellular electron utilization by the acetogen. Here we verified that *Clostridium autoethanogenum*, an industrially relevant acetogen, could use electrons generated from size- and structure-controlled chemically synthesized cadmium sulfide nanoparticles displayed on the cell surface under light-exposure conditions. In addition, transcriptomic analysis showed that the electrons generated from nanoparticles were largely transported to the intracellular matrix via the metal ion or flavin-binding proteins. These results illustrate the potential to increase the CO_2-fixing efficiency of nanoparticle-based artificial photosynthesis by engineering cellular processes related to electron transfer generated from the cathode.

Author contributions: B.-K.C. designed research; S.J., Y.J., M.S.J., J.S., Y.S., S.K., J.B., and S.C. performed research; S.J., S.C., J.-K.L., D.R.K., and B.-K.C. analyzed data; and S.J., S.C., and B.-K.C. wrote the paper.

The authors declare no competing interest.

This article is a PNAS Direct Submission.

This open access article is distributed under Creative Commons Attribution-NonCommercial-NoDerivatives License 4.0 (CC BY-NC-ND).

[1]To whom correspondence may be addressed. Email: bcho@kaist.ac.kr.

This article contains supporting information online at https://www.pnas.org/lookup/suppl/doi:10.1073/pnas.2020552118/-/DCSupplemental.

Published February 22, 2021.

Results

Synthesis and Characterization of CdS-NPs. We sought to develop an artificial photosynthesis system by integrating chemically synthesized CdS-NPs with an acetogenic bacterium, *C. autoethanogenum*. CdS is a photoresponsive semiconductor that can generate electron–hole pairs on receipt of sufficient light intensity to overcome the band gap energy (27, 28). The electrons transferred to the conduction band region move to the electron acceptor region based on the energy potential, and the generated hole in the valence band region accepts electrons from other electron donors (Fig. 1*A*). To apply CdS-NPs to artificial photosynthesis systems, it is critical to increase the electron–hole pair generation rate, whose efficiency varies greatly depending on the size or structure of the CdS-NPs. To this end, we synthesized two kinds of CdS-NPs using two different chemical methods (*Materials and Methods*) and compared their electron–hole pair generation efficiency.

To confirm the structures of the two CdS-NPs, we first performed X-ray diffraction analysis; the results showed that CdS-NP-1 and CdS-NP-2 had cubic and hexagonal structures, respectively (Fig. 1*B*) (27, 28). To investigate the wavelength of light absorbed by each CdS-NP, we measured the absorbance spectrum of the two nanoparticles using spectroscopy. The band gaps of CdS-NP-1 and CdS-NP-2 were 2.62 eV and 2.36 eV, respectively. Therefore, we confirmed that CdS-NP-1 generates electron–hole pairs by absorbing light with an energy of 2.62 eV (473 nm, blue light). In contrast, CdS-NP-2 was confirmed to absorb light with an energy of 2.36 eV (525 nm, green light) to create electron–hole pairs (Fig. 1*C*). Finally, we also determined the number of electron–hole pairs generated by each CdS-NP. To achieve this, we compared their electron–hole pair generation rates by measuring the photocatalytic degradation efficiency using Congo red. When CdS-NPs generate electron–hole pairs, hydroxyl radicals are generated by the flow of electrons, leading to the degradation of Congo red (Fig. 1*D*). After 60 min of light treatment, when the CdS-NP-1 and Congo red were treated together, most of the Congo red had degraded. However, in the case of CdS-NP-2, most of the Congo red was intact (Fig. 1*E* and *SI Appendix*, Fig. S1*A*). Moreover, photoluminescence spectra showed that CdS-NP-1 has a lower electron–hole recombination rate than CdS-NP-2, indicating more photoexcited electrons can be used for photochemical reactions (*SI Appendix*, Fig. S1*B*) (19, 29). In addition, CdS-NP-1 was more favorable for transferring photoexcited electrons to acetogenic bacteria with more a negative conductive edge than that of CdS-NP-2 (*SI Appendix*, Fig. S1*C*) (30). Based on the higher electron–hole pair generation rate, we decided to use CdS-NP-1 to develop an artificial photosynthesis system with *C. autoethanogenum* (CdS-CA hybrid system).

Artificial Photosynthesis Using the CdS-CA Hybrid System. To investigate whether *C. autoethanogenum* utilizes electrons derived from light-exposed CdS-NP-1 for its autotrophic growth, we attempted to attach 0.28 mg L^{-1} of CdS-NP-1 to the outer cell membrane of *C. autoethanogenum*. After cell growth in the midexponential phase with CdS-NP-1, we used scanning electron microscopy to confirm that CdS-NP-1 was displayed on the outer cell surface (Fig. 2*A*); CdS-NP-1 successfully attached to the outer surface of *C. autoethanogenum*, similar to biologically synthesized CdS (18). First, we compared the cell numbers based on the colony-forming units (CFU) of the CdS-CA hybrid system with wild-type cells under light-exposure conditions; the results indicated that the CFU levels were 8.7-fold higher than in wild-type cells (6.00×10^3 vs. 0.69×10^3) (Fig. 2*B*). In general, the CdS-NP can produce H_2 by reducing proton via photoexcited electrons; therefore, we wished to determine whether the photoexcited electrons can be transferred directly to *C. autoethanogenum* or used by photogenerated H_2. To explain our hypothesis, we measured the H_2 generation in the CdS-CA system and confirmed that it produced ~110 nmol H_2 in the PETC medium plus CdS (0.1 mg/mL) condition. In contrast, no H_2 was produced with CdS-CA (*SI Appendix*, Fig. S2). This result illustrates that the CdS-CA hybrid system obtained exogenous

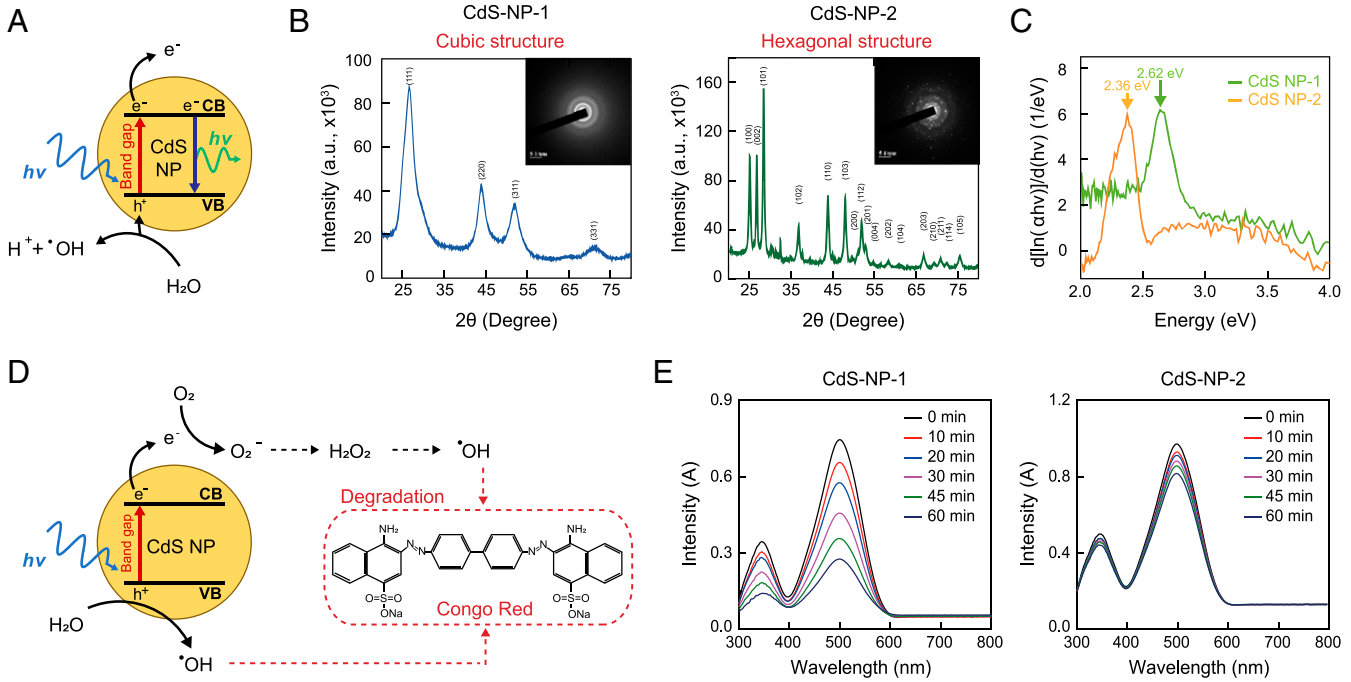

Fig. 1. Physical characterization of the CdS-NP. (*A*) Physical properties of CdS-NP; mechanism of electron–hole pair generation by light. (*B*) X-ray diffraction patterns of the two types of CdS-NPs. (*C*) Measurement of band gap energy for the two types of CdS-NPs. (*D*) Scheme of photocatalytic degradation using Congo red. (*E*) Measurement of photocatalytic degradation of the two types of CdS-NPs.

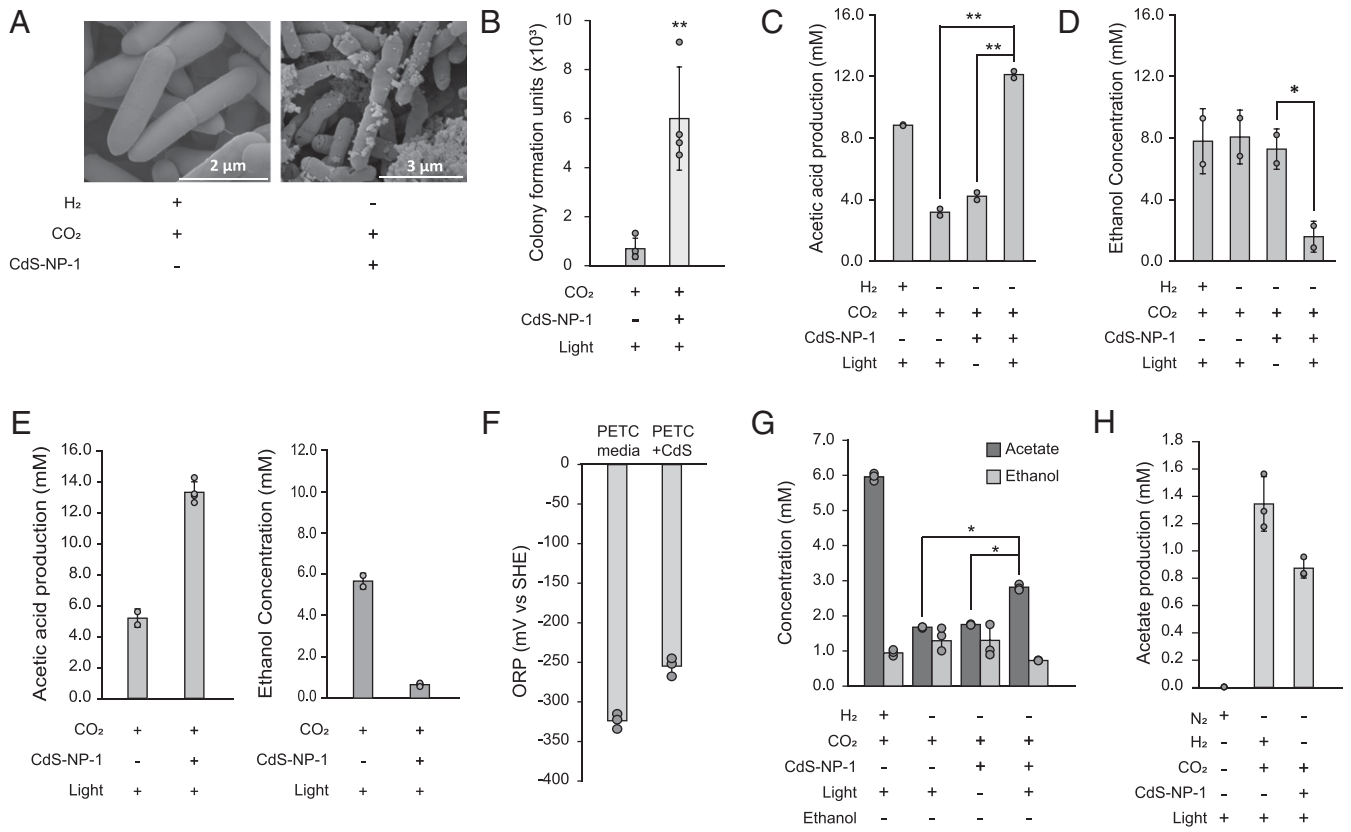

Fig. 2. Productivity behavior of the CdS-CA hybrid system. (*A*) Observation of scanning electron microscope images of the CdS-CA hybrid system. (*B*) Measurement of CFU of CdS-CA under light-exposure conditions. (*C* and *D*) Production of acetate (*C*) and consumption of ethanol (*D*) under the CdS-CA hybrid system. (*E*) Production of acetate (*Left*) and consumption of ethanol (*Right*) of biosynthesis CdS-CA under light-exposed condition. (*F*) Measurement of ORP values in empty PETC medium plus CdS-NP-1. (*G*) Measurement of acetate production using ethanol-removing medium under the CA hybrid system. (*H*) Production of acetate by resting cells under the H_2- or CdS-driven autotrophic condition. Error bars indicate SD. $^*P < 0.05$; $^{**}P < 0.01$, Student's *t* test.

electrons from CdS-NP-1 on the cell surface with light irradiation for autotrophic cell growth.

We next determined whether the CdS-CA hybrid system produces acetate from CO_2 under photoautotrophic conditions. To this end, we analyzed metabolites produced by the CdS-CA hybrid system grown under light-exposure and light-deficient conditions for 72 h. For comparison, the wild-type cells were cultured under energy-deficient (CO_2 only) and H_2-driven autotrophic conditions (CO_2 + H_2) without CdS-NP-1. Note that *C. autoethanogenum* converts CO_2 to acetate by utilizing electrons from hydrogen under H_2-driven autotrophic conditions. The CdS-CA hybrid system produced 12.1 mM acetate under light-exposure conditions, which was 3.8-fold higher than that produced under light-deficient conditions and 2.8-fold higher than that produced under energy-deficient conditions. Under H_2-driven autotrophic conditions, *C. autoethanogenum* produced 8.8 mM acetate (Fig. 2*C*). Thus, the CdS-CA hybrid system converts CO_2 to acetate under photoautotrophic conditions.

Unexpectedly, we observed that ethanol was dramatically consumed by the CdS-CA hybrid system under light-exposure conditions only (Fig. 2*D*). Ethanol was used to solubilize lipoic acid in the culture medium. To prove whether ethanol utilization was mediated by CdS-NP-1, we prepared biologically synthesized CdS-displayed cells using $CdCl_2$ treatment and cultured the cells under light-exposure conditions (*SI Appendix*, Fig. S3). The cells also showed ethanol oxidation under light-exposure conditions (Fig. 2*E*). *C. autoethanogenum* is known to change biomass formation and metabolism by recognizing changes in the redox environment (31); therefore, we hypothesized that changes in the redox environment via CdS-NPs induce a metabolic shift of *C. autoethanogenum*. In fact, the redox environment of the PETC medium with CdS-NP-1 under light-exposure conditions increased the oxidation-reduction potential (ORP) by ∼+30 to 40 mV compared with the PETC medium only (Fig. 2*F*). Therefore, *C. autoethanogenum* oxidizes ethanol because of the redox-dependent metabolic shift when using the extracellular electron supply in *C. autoethanogenum* (31). To verify the acetate production from CO_2 using the CdS-CA hybrid system, we replaced ethanol with distilled water in the culture medium. In the absence of ethanol, acetate production increased by 1.7-fold under the light-exposure conditions compared with under the energy- or light-deficient conditions (Fig. 2*G*). Additionally, we performed a resting cell assay of *C. autoethanogenum* under N_2, CO_2 + H_2, or CO_2 + CdS-NP-1 conditions; the results showed that the cells produced ∼1.2 mM and 0.8 mM acetate under CO_2 + H_2 and CO_2 + CdS-NP-1 conditions, respectively, but no acetate under N_2 conditions (Fig. 2*H*). Taken together, these results indicate that the CdS-CA hybrid system produces acetate from CO_2 using electrons derived from light-activated CdS-NP-1.

Measurement of NADH/NAD$^+$ or NADPH/NADP$^+$ Ratio in the CdS-CA Hybrid System. We observed the oxidation of ethanol using the CdS-CA hybrid system under light-exposure conditions. Based on this, we hypothesized that the CdS-CA hybrid system can obtain NADH or NADPH from ethanol consumption, which could be utilized for acetate and biomass production under these conditions (*SI Appendix*, Fig. S4). To this end, we cultured cells in the presence or absence of 10 mM ethanol under H_2,

CdS-NP-1, and H_2 + CdS-NP-1 conditions. This resulted in an increase in acetate production by ∼1.5-, 2.9-, and 1.6-fold, respectively, compared with the absence of ethanol. Furthermore, we confirmed that the cells consumed ∼7.3 and 4.5 mM ethanol under CdS-NP-1 and H_2 + CdS-NP-1 conditions, respectively, but no ethanol under H_2 conditions (Fig. 3*A*). In addition, biomass formation was increased by 1.3-, 7.0-, and 2.4-fold under the H_2, CdS-NP-1, and H_2 + CdS-NP-1 conditions, respectively, by the addition of ethanol to the culture medium (Fig. 3*B*). These results show that the cells oxidized ethanol when the redox potential was shifted to the oxidized environment by CdS-NP-1, resulting in the enhancement of acetate production and biomass formation. In fact, the redox potential of the CdS-CA hybrid system in the absence of ethanol increased by approximately +30 to 40 mV ORP compared with the control conditions. However, in the presence of ethanol, the ORP value was similar to that under the control condition due to ethanol oxidation (Fig. 3*C*).

We next measured the NADH/NAD and NADPH/$NADP^+$ ratios from three different culture conditions in the presence or absence of ethanol. Unexpectedly, in the presence of ethanol, we observed that the NADH/NAD^+ ratio was decreased by ∼1.5-, 2,1-, and 2.4-fold under the H_2, CdS-NP-1, and H_2 + CdS-NP-1 conditions, respectively (Fig. 3*D*). In contrast, the NADPH/$NADP^+$ ratio was increased by ∼1.8- and 2.5-fold in the presence of ethanol under the CdS-NP-1 and H_2 + CdS-NP-1 conditions, respectively, but decreased by 0.5-fold in the presence of ethanol under the H_2 condition (Fig. 3*E*). Collectively, the CdS-CA hybrid system reduced CO_2 through acetogenesis in the absence of ethanol and obtained additional NADPH through ethanol oxidation under light-exposure conditions. These redox energies could be utilized for an increase in biomass. In addition, when two types of energy sources were used together (i.e., under the H_2 + CdS-NP-1 condition), the cellular NADH or NADPH levels were increased compared with those under either H_2 or CdS-NP-1 only. This suggests that the H_2 + CdS-NP-1 culture condition is beneficial for biomass formation or chemical production using *C. autoethanogenum*.

Transcriptional Analysis of the CdS-CA Hybrid System under Autotrophic Conditions. To understand the transcriptional changes of the CO_2 fixation-related genes in response to the autotrophic conditions, we performed RNA-sequencing (RNA-seq). To select RNA sampling points, we measured both acetate production and ethanol consumption according to the growth phases of *C. autoethanogenum* under CdS- and H_2-driven autotrophic conditions. Acetate production and ethanol consumption of the CdS-CA hybrid system

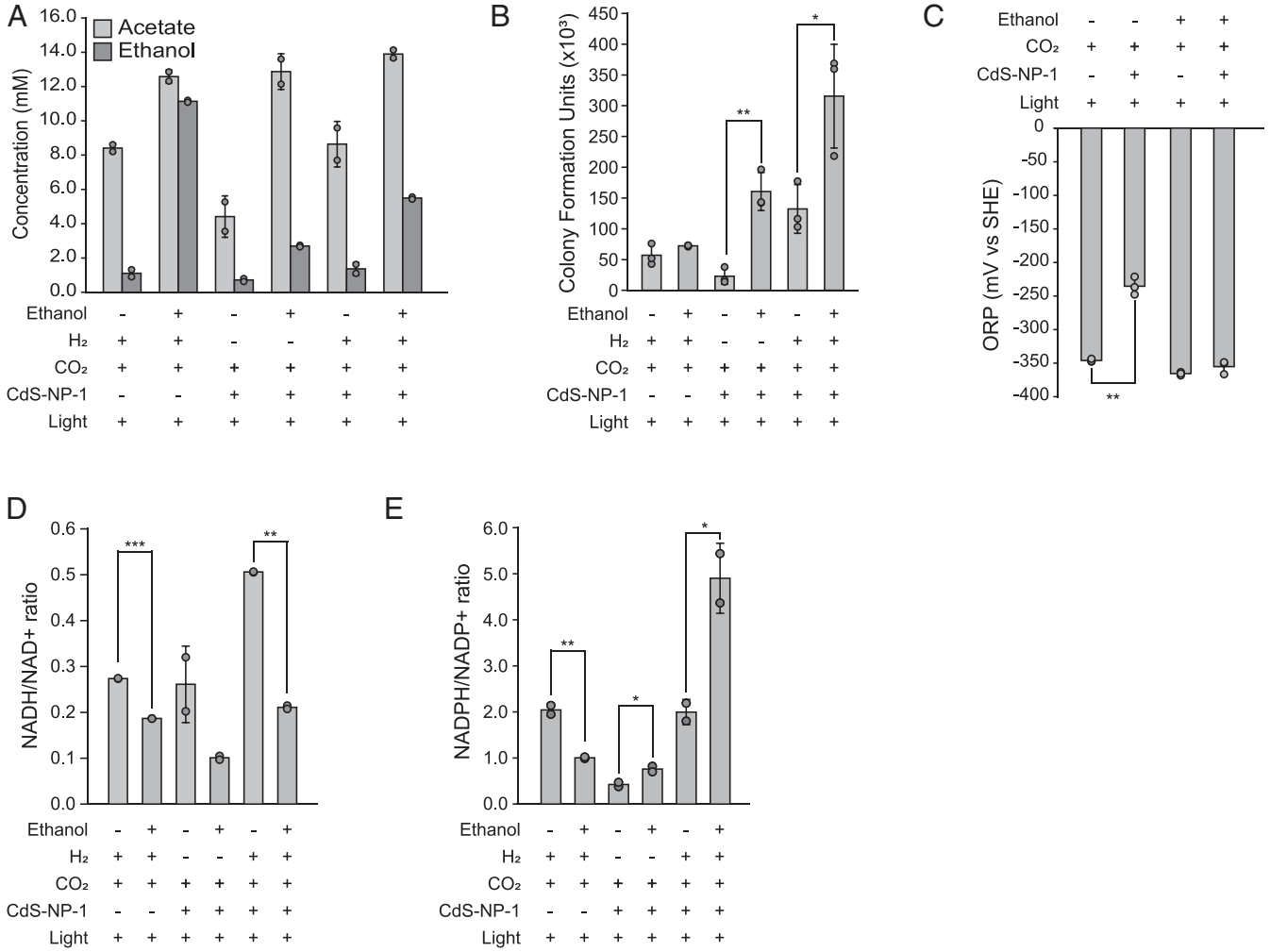

Fig. 3. Phenotype analysis of *C. autoethanogenum* in the presence of ethanol under H_2-, CdS-NP-1–, or H_2 + CdS-NP-1–driven autotrophic conditions. (*A*) Production of acetate or consumption of ethanol by *C. autoethanogenum*. (*B*) Measurement of CFU. (*C*) Measurement of ORP values in the CdS-CA hybrid system in with or without ethanol conditions. (*D*) Measurement of the NADH/NAD^+ ratio. (*E*) Measurement of the NADPH/$NADP^+$ ratio. Error bars indicate SD. **P* < 0.05; ***P* < 0.01; ****P* < 0.001, Student's *t* test.

were increased after 28 h, which reached the highest levels at 44 h and then were completed after 68 h (*SI Appendix*, Fig. S5*A*). As a control, we prepared heterotrophic cultures of *C. autoethanogenum* using fructose as the sole carbon and energy source (*SI Appendix*, Fig. S5*B*). The RNA-seq of cells at the midexponential phase generated a total of 4.3 to 10.5 million sequence reads mapped to the reference genome (NC_022592.1) with at least 100-fold coverage (Dataset S1). Hierarchical clustering and principal component analysis of the sequencing results demonstrated significant and reproducible differences in gene expression between the growth conditions (*SI Appendix*, Fig. S5 *C* and *D*). RNA-seq data were then normalized by DESeq2 to compare transcript levels under the growth conditions (32). More than 2,768 genes showed a normalized expression value of ≥10 across all growth conditions, reflecting the transcription of 68% of the annotated genes under at least one condition (Dataset S2).

In brief, changes in transcript levels of genes involved in the glycolysis/gluconeogenesis pathway were similar under H_2- and CdS-driven autotrophic conditions (*SI Appendix*, Fig. S6 and Dataset S3). For example, a gene encoding glyceraldehyde-3-phosphate dehydrogenase was up-regulated by ∼2.0-fold (DESeq $P < 1.75 \times 10^{-42}$) and 2.6-fold (DESeq $P < 1.33 \times 10^{-69}$) under the two autotrophic growth conditions, respectively, compared with heterotrophic growth (33). The genes associated with the WL pathway were highly expressed with similar expression levels (*SI Appendix*, Fig. S6 and Dataset S3). Based on the comparison of the transcript profiles in the carbon metabolism pathway, we confirmed similar transcriptional profiles of many genes associated with autotrophic growth between H_2- and CdS-driven autotrophic conditions compared with heterotrophic growth. Interestingly, the genes encoding the energy conservation system were more highly expressed under the CdS-driven autotrophic condition than under the H_2-driven autotrophic condition. In particular, genes encoding the Rnf complex, which is essential for energy conservation by coupling ferredoxin oxidation with NAD^+ reduction and then producing a proton gradient across the membrane in acetogenic bacteria, were up-regulated with a minimum fold change of 1.6 (DESeq $P < 5.68 \times 10^{-28}$) for the *rnfC* gene under the CdS-driven autotrophic condition compared with the H_2 condition. In addition, genes encoding hydrogenases were up-regulated. Among them, Ni/Fe hydrogenase genes were ∼3.8-fold up-regulated (DESeq $P < 1.36 \times 10^{-3}$) under the CdS-driven autotrophic condition, consistent with the increased enzyme activity of Ni/Fe hydrogenase in the *M. thermoacetica* CdS system (21) (*SI Appendix*, Fig. S6 and Dataset S3). This means that hydrogenase is highly active in CdS-NP condition because photo-semiconductors produce H_2 via transfer of photoexcited electrons to protons under light conditions. Based on the transcriptome profiles of carbon and energy metabolism, we concluded that the CdS-CA hybrid system reduces CO_2 to acetate using the acetogenesis pathway for its autotrophic growth, which includes the WL pathway, hydrogenases, and the Rnf complex.

Energy Metabolism between CdS- and H_2-Driven Autotrophic Conditions. We observed different transcriptional levels of genes related to energy metabolism between the two autotrophic conditions. This result indicates that the process of accepting electrons generated from CdS-NP-1 under light-exposed conditions was quite different from that of accepting electrons generated from H_2. To identify significantly altered genes between the two autotrophic conditions, we isolated differentially expressed genes (DEGs) by $\log_2$(FC) >1.0 or <–1.0, with adjusted $P < 0.01$. Under the CdS-driven autotrophic condition, 763 genes were up-regulated and 679 genes were down-regulated compared with the H_2-driven autotrophic condition (Fig. 4*A* and Dataset S4). Classification of those DEGs according to Clusters of Orthologous Groups of proteins (COG) categories showed that "energy production and conservation (C)" were highly conserved (Fig. 4*B*). This result suggests that energy metabolism under the CdS-driven autotrophic condition is potentially different from that under the H_2-driven autotrophic condition.

Interestingly, Gene Ontology (GO) term analysis of the up-regulated genes in category C showed a common feature of "metal ions" or "flavin binding" (Fig. 4*C*). These cofactors act as electron acceptors and are involved in electron transfer in gram-positive bacteria (12–14). Therefore, we hypothesized that the expansion of cofactor pools, such as metal ions or flavin, could increase the CO_2 fixation rate of *C. autoethanogenum* under CdS-driven autotrophic conditions. To verify this, we measured the acetate production of the CdS-CA hybrid system with the addition of metal ions or flavin molecules. First, we supplied 10 μM of metal ions to the CdS-CA hybrid system and found no significant difference in acetate production compared with the nontreated condition (Fig. 4*D*). Then we supplied 10 μM riboflavin or 5 μM FMN to the CdS-CA hybrid system. Interestingly, when both iron and FMN were treated together, acetate production was increased by ∼2.0-fold compared with the CO_2 + CdS condition (Fig. 4*E*). To support our hypothesis that cofactors will play an important role in the electron transfer process in the CdS-CA system, we conducted photocatalyst experiments using Congo red with Fe + FMN mediator in distilled water. If the decomposition amount of Congo red decreases, the mediator can accept the electron from the CdS, and transfer into the cell. The degradation rate of Congo red was decreased by ∼40% with the mediator compared to without the mediator (*SI Appendix*, Fig. S7). This result supports the hypothesis that electrons generated from CdS can be transferred to *C. autoethanogenum* indirectly as electrons are transferred to mediators such as Fe + FMN in medium.

Based on these results and the absence of cytochrome *c* in *C. autoethanogenum*, three electron transfer mechanisms are possible with the CdS-CA hybrid system (*SI Appendix*, Fig. S8). First, the fact that transcription levels of iron transporters were up-regulated under the CdS-driven autotrophic condition compared with levels under the H_2-driven autotrophic condition suggests an indirect EET mechanism mediated by metal ions such as Fe^{2+}/Fe^{3+} (*SI Appendix*, Fig. S9). The metal ions can accept light-inducing electrons from the CdS-NPs, which can be transferred to the cells by iron transporters. Second, we found a transcriptionally activated candidate gene (CAETHG_RS11680) as a homologous protein of the RibU riboflavin transporter, which contains highly conserved amino acid residues that form hydrogen bonds with riboflavin (*SI Appendix*, Fig. S10) (13, 34, 35). The riboflavin treatment experiments also support the role of the riboflavin transporter in electron transport. Finally, the electrons generated by the CdS attached to the bacterial surface can be directly transferred by the Fe-S cluster, an electron transfer chain within membrane-bound proteins. The transcription levels of membrane-bound electron-bifurcating NADP- and ferredoxin-dependent [FeFe]-hydrogenase with formate dehydrogenase (CAETHG_RS13725-13770) complex were up-regulated under the CdS-driven autotrophic condition. In addition, the Rnf complex with the Fe-S cluster, the most crucial electron transfer membrane protein complex in *C. autoethanogenum*, was highly up-regulated (*SI Appendix*, Fig. S6). Considering these findings together, we concluded that genes encoding the proteins requiring cofactors as electron acceptors were up-regulated in *C. autoethanogenum* under the CdS-driven autotrophic condition, and that these cofactors could support the enhancement of CO_2 fixation in *C. autoethanogenum* by transferring electrons generated from CdS-NP-1 under light-exposed conditions.

Discussion

In this study, we constructed an artificial photosynthesis system using an industrially relevant acetogenic bacterium, *C. autoethanogenum*, with a chemically synthesized CdS nanoparticle,

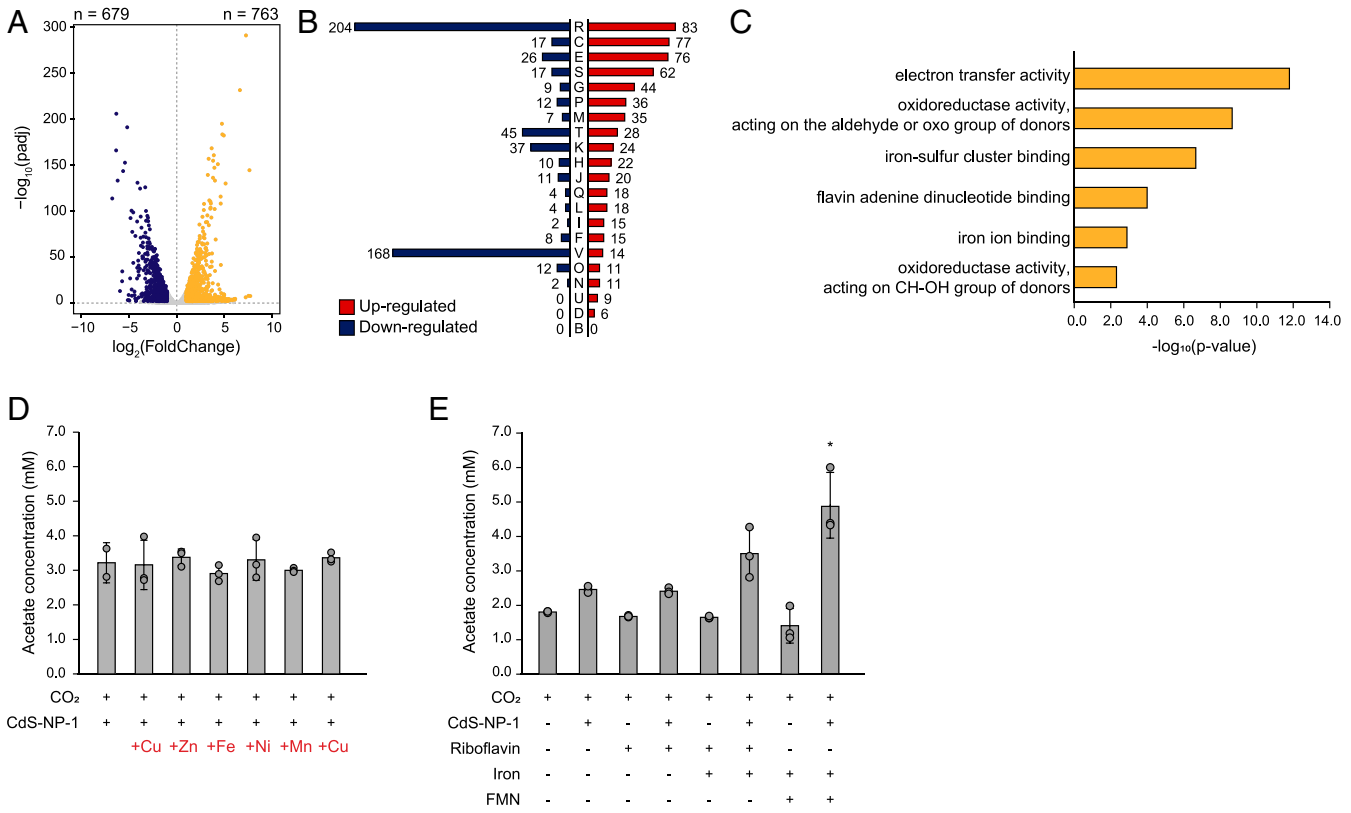

Fig. 4. DEG analysis between the CdS and H_2 autotrophic conditions. (*A*) Volcano plots showing the up-regulated and down-regulated genes by DEG analysis between the CdS and H_2 autotrophic conditions. (*B*) Classification of COG categories in up-regulated and down-regulated genes. (*C*) Classification of the molecular function of GO enrichment analysis of COG "C: energy production and conversion." (*D*) Measurement of acetate production under treatment with several metal ions. (*E*) Measurement of acetate production under the iron with riboflavin or FMN treatment condition. Error bars indicate SD. $*P < 0.05$, Student's *t* test.

CdS-NP-1. Occasionally, the in vivo biosynthesis of photoresponsive semiconductors harms bacterial metabolism, owing to the cellular detoxification mechanism (36). In addition, their electron–hole pair generation efficiency varies considerably, depending on their size and structure, but bacterial biosynthesis has no selectivity for the size and structure of semiconductors. To overcome these limitations, we synthesized photoresponsive semiconductors in vitro and localized them to the bacterial cell surface. The resulting CdS-CA hybrid system autotrophically produced 0.8 mM acetate under light-exposure conditions.

Transcriptome analysis demonstrated that most of genes involved in the WL pathway and energy conservation, including the Rnf complex, were significantly up-regulated, similar to those under the H_2-driven autotrophic condition. Also, genes related to oxidoreductases were up-regulated under the CdS-driven autotrophic condition compared to the H_2-driven autotrophic condition. This phenomenon is related to changes in the cellular redox environment by light activation of the displayed CdS-NP-1, which induces changes in cellular metabolism in *C. autoethanogenum* (31). Interestingly, the CdS-CA hybrid system could obtain NADPH from ethanol oxidation in the oxidized redox environment, resulting in a dramatic increase in the biomass and recovery of the reduced redox environment. In addition, when two energy sources of H_2 and CdS were used together, acetate production and the $NADH/NAD^+$ or $NADPH/NADP^+$ ratio were increased. These results show that the use of H_2 and CdS together could complement the low solubility of H_2 with another energy source from light-activated CdS and could increase the cellular NADH or NADPH pool. Acetate production was also increased when cofactors, such as metal ions or flavin molecules, were added. Therefore, we suggest that the CdS-CA hybrid system is beneficial for biomass or chemical production in the H_2-driven autotrophic condition.

Unlike carbon metabolism, the energy production and conservation system showed differences between the CdS- and H_2-driven autotrophic conditions. Among the subunits of the Rnf complex, only the RnfB subunit that received electrons from reduced ferredoxin showed higher expression levels in the CdS treatment condition than in the H_2 condition. Under the H_2-driven autotrophic condition, hydrogenase generates both ferredoxin and NADPH from H_2, and the Rnf complex generates NADH by transferring electrons from reduced ferredoxin to NAD^+. In contrast, the extracellular electrons generated from the light-activated CdS-NPs can be transported to the intracellular matrix of *C. autoethanogenum* via metal or flavin molecules and eventually can be transferred to NADH or NADPH as electron donors for cellular metabolism, including CO_2 fixation. Thus, we considered that NAD/NADP-associated oxidoreductase and flavin-associated proteins or flavoproteins are more likely to act as intracellular electron carriers (*SI Appendix*, Fig. S11) (37, 38).

The artificial photosynthesis system using acetogenic bacteria with photoresponsive semiconductors still requires further improvements to increase the efficiency of energy metabolism. For instance, genetic engineering of acetogenic bacteria is necessary to efficiently capture the extracellular electrons for a bifurcating electron transfer system to generate cellular NADH or NADPH pools. It is also necessary to develop an efficient defense mechanism against oxidative stress to maintain the redox balance in the system. Our results provide an artificial photosynthesis

system using *C. autoethanogenum* coupled with a photoresponsive semiconductor, CdS-NP-1, and an engineering strategy for further improvements of the CdS-CA hybrid system.

Materials and Methods

Synthesis and Characterization of CdS-NPs. The synthesis of CdS-NPs was based on the trituration method (27, 28). Detailed information on the synthesis and characterization of CdS-NPs is provided in *SI Appendix, Materials and Methods*.

Bacterial Strains and Growth Conditions. *C. autoethanogenum* DSM 10061 was obtained from the Leibniz Institute DSMZ (German Collection of Microorganisms and Cell Cultures). Cells were cultivated anaerobically at 37 °C in 97 mL of PETC medium. Medium composition, CFU measurement, resting assay, and culture conditions are described in *SI Appendix, Materials and Methods*.

Biosynthesis of CdS-NPs. *C. autoethanogenum* was cultured strictly anaerobically under 100 mL of PETC medium with 5 g/L fructose at 37 °C until an OD_{600} of ∼0.6 to 0.8 was reached. Then 1 mM $CdCl_2$ was added, followed by further incubation at 37 °C for 24 h. Detailed information on the biosynthesis of CdS-NPs is provided in *SI Appendix, Materials and Methods*.

RNA-Seq Library Preparation. The extraction of total RNA from the collected cells and the RNA-seq library construction method are described in *SI Appendix, Materials and Methods*.

Further information on regents, culture conditions, RNA-seq analysis, resting cell assay, NADH/NAD and NADPH/NADP ratio measurements, and ORP value measurement is provided in *SI Appendix, Materials and Methods*.

Data Availability. The data reported in this paper have been deposited in the Gene Expression Omnibus (GEO) database, https://www.ncbi.nlm.nih.gov/geo (accession no. GSE157613).

ACKNOWLEDGMENTS. This work was supported by the Intelligent Synthetic Biology Center of the Global Frontier Project (2011-0031957 to B.-K.C.) and the C1 Gas Refinery Program (2018M3D3A1A01055733 to B.-K.C.) through the National Research Foundation of Korea funded by the Ministry of Science and ICT.

1. H. L. Drake, A. S. Gössner, S. L. Daniel, Old acetogens, new light. *Ann. N. Y. Acad. Sci.* **1125**, 100–128 (2008).
2. Y. Song *et al*., Determination of the genome and primary transcriptome of syngas fermenting Eubacterium limosum ATCC 8486. *Sci. Rep.* **7**, 13694 (2017).
3. Y. Song *et al*., Genome-scale analysis of syngas fermenting acetogenic bacteria reveals the translational regulation for its autotrophic growth. *BMC Genomics* **19**, 837 (2018).
4. K. Igarashi, S. Kato, Extracellular electron transfer in acetogenic bacteria and its application for conversion of carbon dioxide into organic compounds. *Appl. Microbiol. Biotechnol.* **101**, 6301–6307 (2017).
5. D. R. Lovley, K. P. Nevin, Electrobiocommodities: Powering microbial production of fuels and commodity chemicals from carbon dioxide with electricity. *Curr. Opin. Biotechnol.* **24**, 385–390 (2013).
6. K. P. Nevin *et al*., Electrosynthesis of organic compounds from carbon dioxide is catalyzed by a diversity of acetogenic microorganisms. *Appl. Environ. Microbiol.* **77**, 2882–2886 (2011).
7. G. Mohanakrishna, J. S. Seelam, K. Vanbroekhoven, D. Pant, An enriched electroactive homoacetogenic biocathode for the microbial electrosynthesis of acetate through carbon dioxide reduction. *Faraday Discuss.* **183**, 445–462 (2015).
8. K. Rabaey, R. A. Rozendal, Microbial electrosynthesis: Revisiting the electrical route for microbial production. *Nat. Rev. Microbiol.* **8**, 706–716 (2010).
9. J. C. Thrash, J. D. Coates, Review: Direct and indirect electrical stimulation of microbial metabolism. *Environ. Sci. Technol.* **42**, 3921–3931 (2008).
10. E. Marsili *et al*., Shewanella secretes flavins that mediate extracellular electron transfer. *Proc. Natl. Acad. Sci. U.S.A.* **105**, 3968–3973 (2008).
11. S. Kato, Microbial extracellular electron transfer and its relevance to iron corrosion. *Microb. Biotechnol.* **9**, 141–148 (2016).
12. E. Zhang, Y. Cai, Y. Luo, Z. Piao, Riboflavin-shuttled extracellular electron transfer from Enterococcus faecalis to electrodes in microbial fuel cells. *Can. J. Microbiol.* **60**, 753–759 (2014).
13. S. H. Light *et al*., A flavin-based extracellular electron transfer mechanism in diverse gram-positive bacteria. *Nature* **562**, 140–144 (2018).
14. L. Shi *et al*., Extracellular electron transfer mechanisms between microorganisms and minerals. *Nat. Rev. Microbiol.* **14**, 651–662 (2016).
15. L. Shi *et al*., Molecular underpinnings of Fe(III) oxide reduction by Shewanella oneidensis MR-1. *Front. Microbiol.* **3**, 50 (2012).
16. V. A. García-Angulo, Overlapping riboflavin supply pathways in bacteria. *Crit. Rev. Microbiol.* **43**, 196–209 (2017).
17. K. P. Nevin, T. L. Woodard, A. E. Franks, Z. M. Summers, D. R. Lovley, Microbial electrosynthesis: Feeding microbes electricity to convert carbon dioxide and water to multicarbon extracellular organic compounds. *mBio* **1**, e00103-10 (2010).
18. K. K. Sakimoto, A. B. Wong, P. Yang, Self-photosensitization of nonphotosynthetic bacteria for solar-to-chemical production. *Science* **351**, 74–77 (2016).
19. H. Zhang *et al*., Bacteria photosensitized by intracellular gold nanoclusters for solar fuel production. *Nat. Nanotechnol.* **13**, 900–905 (2018).
20. K. K. Sakimoto, S. J. Zhang, P. Yang, Cysteine-cystine photoregeneration for oxygenic photosynthesis of acetic acid from CO_2 by a tandem inorganic-biological hybrid system. *Nano Lett.* **16**, 5883–5887 (2016).
21. N. Kornienko *et al*., Spectroscopic elucidation of energy transfer in hybrid inorganic-biological organisms for solar-to-chemical production. *Proc. Natl. Acad. Sci. U.S.A.* **113**, 11750–11755 (2016).
22. B. Wang *et al*., Enhanced biological hydrogen production from Escherichia coli with surface precipitated cadmium sulfide nanoparticles. *Adv. Energy Mater.* **7**, 1700611 (2017).
23. W. Wei *et al*., A surface-display biohybrid approach to light-driven hydrogen production in air. *Sci. Adv.* **4**, eaap9253 (2018).
24. J. Guo *et al*., Light-driven fine chemical production in yeast biohybrids. *Science* **362**, 813–816 (2018).
25. R. Dunleavy, L. Lu, C. J. Kiely, S. McIntosh, B. W. Berger, Single-enzyme biomineralization of cadmium sulfide nanocrystals with controlled optical properties. *Proc. Natl. Acad. Sci. U.S.A.* **113**, 5275–5280 (2016).
26. Y. Choi, T. J. Park, D. C. Lee, S. Y. Lee, Recombinant Escherichia coli as a biofactory for various single- and multi-element nanomaterials. *Proc. Natl. Acad. Sci. U.S.A.* **115**, 5944–5949 (2018).
27. J. Chen *et al*., Facile synthesis of CdS/C core-shell nanospheres with ultrathin carbon layer for enhanced photocatalytic properties and stability. *Appl. Surf. Sci.* **362**, 126–131 (2016).
28. A. Dumbrava, G. Prodan, D. Berger, M. Bica, Properties of PEG-capped CdS nanopowders synthesized under very mild conditions. *Powder Technol.* **270**, 197–204 (2015).
29. G. Dong *et al*., Cadmium sulfide nanoparticles-assisted intimate coupling of microbial and photoelectrochemical processes: Mechanisms and environmental applications. *Sci. Total Environ.* **740**, 140080 (2020).
30. J. Philips, Extracellular electron uptake by acetogenic bacteria: Does H_2 consumption favor the H_2 evolution reaction on a cathode or metallic iron? *Front. Microbiol.* **10**, 2997 (2020).
31. F. Kracke, B. Virdis, P. V. Bernhardt, K. Rabaey, J. O. Krömer, Redox- dependent metabolic shift in Clostridium autoethanogenum by extracellular electron supply. *Biotechnol. Biofuels* **9**, 249 (2016).
32. M. I. Love, W. Huber, S. Anders, Moderated estimation of fold change and dispersion for RNA-seq data with DESeq2. *Genome Biol.* **15**, 550 (2014).
33. E. Marcellin *et al*., Low carbon fuels and commodity chemicals from waste gases—systematic approach to understand energy metabolism in a model acetogen. *Green Chem.* **18**, 3020–3028 (2016).
34. A. Gutiérrez-Preciado *et al*., Extensive identification of bacterial riboflavin transporters and their distribution across bacterial species. *PLoS One* **10**, e0126124 (2015).
35. P. Zhang, J. Wang, Y. Shi, Structure and mechanism of the S component of a bacterial ECF transporter. *Nature* **468**, 717–720 (2010).
36. K. Helbig, C. Grosse, D. H. Nies, Cadmium toxicity in glutathione mutants of Escherichia coli. *J. Bacteriol.* **190**, 5439–5454 (2008).
37. J. Liu *et al*., Metalloproteins containing cytochrome, iron-sulfur, or copper redox centers. *Chem. Rev.* **114**, 4366–4469 (2014).
38. F. Kracke, I. Vassilev, J. O. Krömer, Microbial electron transport and energy conservation—the foundation for optimizing bioelectrochemical systems. *Front. Microbiol.* **6**, 575 (2015).